PAPER

Check for updates

Thermal insulation properties of lightweight, self-healing, and mesoporous carrageenan/PMMA cryogels†

Akbar Mirzaei,[a] Shahrzad Javanshir [iD] *[a] and Peyman Servati[b]

The development of new bio-based cryogel materials with low environmental impact and various properties such as self-healing, flame-retardancy, low thermal conductivity has emerged as a cutting-edge research topic in special-purpose materials and a significant challenge. Herein, we report a simple processing methodology for preparing new mesoporous light weight thermal insulation biomass hybrid cryogels based on natural and biocompatible polymers, including marine glycosaminoglycan carrageenan moss (CM) and polymethyl methacrylate (PMMA) abbreviated as CM/PMMA under cryo conditions. The mechanical, thermal, and physicochemical characterization of the obtained hybrid cryogel was studied. The effect of increasing thickness on thermal conductivity and compressive strength was investigated. The results show that the thermal conductivity increases from 0.068 W m^{-1} K^{-1} to 0.124 W m^{-1} K^{-1} with increasing thickness. Also, the compressive strength changed from 89.5% MPa to 95.4% MPa. The results revealed that cryogel has a wrinkled surface and interconnected pores and exhibits high flexibility, self-healing ability, flame retardancy, and low thermal conductivity.

1 Introduction

Three-dimensional porous materials such as aerogels and cryogels with remarkable physicochemical properties such as low density, high specific surface area, and low thermal conductivity are promising materials for insulation.[1–6] Among the types of aerogels and cryogels, melamine–formaldehyde aerogels, silica (SiO$_2$) aerogels and nano-porous silica cryogel,[3,7–9] silica aerogel-filled PMMA,[10,11] and carbon-based aerogel,[12] carbon aerogels based on bacterial cellulose[1] are some of the most popular porous unnatural materials for insulation. However, the use of these materials has some disadvantages. For example, although silica aerogels are very light weight and super-insulating materials, their fragility hinders their practical use. Hence the idea of using bio-aerogels made from natural polymers, such as cellulose, carrageenan (CG), pectin, starch and polysaccharides has been formed. The development of polysaccharide-based aerogels, which are more resistant and green, could solve this problem.[13]

The name carrageenan is attributed to a family of hydrophilic sulfated polysaccharides, the most widely known marine glycosaminoglycans (GAGs) with high-molecular-weight obtained from red seaweeds, and are capable of forming a porous thermo-reversible gel with self-healing features.[14] Carrageenan-based aerogels have gained significant importance in recent eras owing to their biocompatibility, high viscosity, and gelling capability, not only in the food industry but also in medical, pharmaceutical, and biotechnological research. The production of carrageenan aerogel through chemical and physical cross-linking been reported very recently.[15,16] Dual physical and chemical cross-linking of κ-carrageenan was found to be indispensable for the improved stability in water and mechanical properties of the carrageenan hydrogel network.[17]

Properties such as biocompatibility,[18–20] high-temperature resistance, chemical stability, exceptional optical clarity, excellent weatherability and excellent mechanical properties[19–21] have made PMMA a polymer of choice for composites aerogels with improved mechanical and thermal properties. Recently, the preparation of silica aerogels composites using PMMA polymer as reinforcement for thermal insulation materials been reported.[22–24]

Thermal insulation materials, serving as a barrier, can efficiently prevent temperature-gradient induced heat transfer so the use of these materials in the field of packaging, construction, and energy storage seems essential. Since low-energy buildings require materials with low thermal conductivity and high fire retardant, thermal insulation has become prevalent.[1,25–29] Unfortunately, insulators based on traditional organic materials are flammable, and inorganic insulators suffer from high thermal conductivity and fragility. Although

[a]*Pharmaceutical and Heterocyclic Compounds Research Laboratory, Chemistry Department, Iran University of Science and Technology, Tehran, Iran*

[b]*Department of Electrical and Computer Engineering, University of British Columbia, Vancouver, BC V6T 1Z4, Canada. E-mail: ak_mirzaei@chem.iust.ac.ir; peymans@ece. ubc.ca; shjavan@iust.ac.ir; Tel: +98-21-77240516*

adding phosphorus and halogen compounds to polymers reduces flammability, they are hazardous to human health and the environment due to their limited biodegradation.[30–37] Therefore, providing flexible and flame-retardant materials with low thermal conductivity based on natural and unnatural polymers is an essential requirement. Furthermore, service life and durability are essential parameters for the thermal insulators to estimate their applications. All artificial materials end up getting damaged. Damaged parts must then be replaced, which is costly. The stability and durability of the materials can be increased by repairing the damages in an autonomic way. Therefore, it is desirable to develop a mechanically robust thermal insulator possessing the self-healing ability to not only prolong the service life of the materials but also increase the durability and the reliability of the thermal insulator in specific applications by avoiding the accumulation of cracks or damages.[38,39] Until now, many self-healing hydrogels and cryogels based on polymers such as chitosan, cellulose, and PVA been developed.[40–42]

In this research, a light weight, flexible mesoporous hybrid cryogel with low thermal conductivity, self-healing ability, and flame retardancy based on natural polysaccharide CM and PMMA was prepared utilizing simple processes. We have consolidated all the merits into a single flame retardant mesoporous cryogel, which is environmentally friendly, inexpensive, and can be easily replicated. The dual cross-linking, including chemical and electrostatic interaction were used to prepare of CM/PMMA cryogels with improved mechanical properties and stability for thermal insulation applications.

2 Experimental

2.1 Material and method

PMMA was purchased from Aldrich. The CM (*Chondrus crispus*, Angel Brand) was purchased from the grocery store. Carrageenan contained a mixture of κ and λ having a weight-average molecular weight of >200–800 kDa, and the only hydrolysis product is galactose. The ratio of κ : λ varies by season and location from about 90 : 10 to about 60 : 40 with a typical average of about 75 : 25 (ref. 43).

FT-IR (Shimadzu 8400 S), FE-SEM (Nova NanoSEM450) and XRD (D8 Advance Sol-X, Bruker Co., Germany) were used to study the structure and morphology of produce. Device was used to investigate thermal insulation properties. The Mixer Mill MM 400 was used for ball milling.

2.2 Grafting of PMMA and CM and preparation of hybrid cryogel

CM (2 g) was washed several times with distilled water to remove the salts, then dried at 60 °C for 24 h. The dried CM was ball milled for 5 minutes at 30 Hz. Next, 0.5 g of powdered CM was dissolved in water (30 ml) at 60 °C. To the resulting solution, KI (0.5 g, 3 mmol) as a cross-linking agent was added under stirring, followed by the addition of a solution of PMMA (0.1 g) in chloroform (30 ml). The obtained gel was lyophilized

at −50 °C, and the obtained cryogel was then washed several times to remove the residual of KI and dried at 50 °C.

2.3 Characterization

The FTIR, UV-vis, XRD and SEM were used to characterize the hybrid cryogel structure and morphology. The thermal stability was determined by thermogravimetric analysis (TGA) at the temperature range of 25–800 °C under the atmosphere of argon and oxygen. The specific surface area and the pore size distribution of hybrid cryogel were obtained from the adsorption/desorption isotherm by applying the Brunauer–Emmett–Teller (BET) theory through an automatic surface area analyzer at N_2 environment.

2.4 Non-automatic self-healing CM/PMMA hybrid cryogel

Non-autonomic self-healing hydrogels can recover their original and permanent form under the effect of an external stimulating signal, such as heat, light, or an electric field. Stimulus-sensitive hydrogels can sense an external stimulus, evaluate it and react accordingly. In other words, they have a sensor, processor, and trigger functions and are considered as 'smart cryogel'.[44–46] The self-healing ability of the CM/PMMA hybrid cryogel, was studied by direct visual observation method. First, two circular samples of diameter equal to 4 cm, impregnated with rhodamine B and methylene blue, were separated into two semicircular (or semi-square) pieces. The semicircular pieces of hybrid cryogel were assembled, and the self-healing efficiency was observed at 40 °C and recorded by optical microscopy images. Rapid self-healing was observed, and micro-crack by the hydrogel site were filled after 15 min. The recovered hybrid cryogel could tolerate its weight and withstand stretching without further impairment. The details of the self-healing process were recorded by optical microscopy (microscope primo star zeiss).

2.5 Mechanical properties

The compression properties of the CM/PMMA hybrid cryogel were analyzed using JINJIAN Universal Testing Machine type: XWW-20 compressive tests were all conducted on a cylindrical sample (36 mm in diameter and 8.90 and 4.45 mm in height). Afterward, it was placed on the lower plate of the instrument and compressed with a probe at a strain rate of 1 mm min^{-1} at room temperature (25 °C) in air. Furthermore, the density of the three cryogels was measured.

2.6 Swelling test

The swelling degree of prepared hybrid cryogel was determined *via* soaking of a hybrid cryogel in 50 ml of distilled water at 20 °C to 60 °C. The swelling degree (SD%) at equilibrium was calculated using eqn (1). Where M_0 is the dry cryogel weight (g), and M_1 is the swollen cryogel weight (g).

$$\text{SD} = (M_1 - M_0) \times 100/M_0 \tag{1}$$

2.7 Thermal conductivity and flammability tests

Thermal conductivity k of the sample was calculated using Fourier's law of heat conduction expressed as:

$$K = (Q \times L)/(A \times (T_2 - T_1)) \tag{2}$$

Q is the heat-transfer rated in watts (W), T_2 and T_1 are temperatures of the heating and cooling stage, L is the sample thickness, and A is the surface area.[47] Thermal conductivity (k) of CM/PMMA hybrid cryogel samples with a diameter of 2.5 cm and different thicknesses (2.22 mm, 3.22 mm, and 4.22 mm) was evaluated using a linear heat conduction PA Hilton. The standard uncertainty in the measurement of thermal conductivity is ±0.01 W m^{-1} K^{-1}.

Typical fire resistance is based on the intrinsic flame retardant performance of the materials, such as high decomposition temperature, suitable thermal insulation property and the formation of charcoal after burning. Highly porous materials forming a large amount of char logically exhibit better performance in terms of fire resistance, *i.e.* reduced smoke and toxic gas emissions, longer ignition time, and slower flame spread.[12,48] Flammability test was carried out on CM/PMMA hybrid cryogel with a thickness of 4.22 mm using the horizontal burning test.

2.8 Viscosity measurements

The viscosity of the CM solution (16.67 g L^{-1}) was determined by a digital viscometer (PolyVISC®-Type L). The standard spindle SP2 with a shear rate 100 rpm was used for determination of viscosity at 20, 25 and, 50 °C.

3 Results and discussion

3.1 FTIR spectroscopy of PMMA/CM hybrid cryogel

The schematic pathway and FTIR spectra of CM/PMMA hybrid cryogel, CM, and PMMA are shown in Fig. 1 and 2. The asymmetric and the symmetric stretching bands of CH$_2$ group in PMMA appear at 2999 and 2954 cm^{-1}, respectively (Fig. 2). An additional small peak at 2856 cm^{-1} is due to –CH$_3$ stretching vibrations.[49,50] Moreover, the sharp absorption band that appeared at 1735 cm^{-1} is related to the ester carbonyl C=O stretching vibration in PMMA. Medium intensity bands at 1276 cm^{-1}, 1245 cm^{-1} and 991 cm^{-1} are assigned to C–O stretching modes,[51] and the absorption at 1149 cm^{-1} is related to the C–O–C stretching vibration bonds of the ester group in PMMA.[52] The absorption bond at 1487 cm^{-1} could be ascribed to the deformation vibration of –CH$_3$ (ref. 50, 53 and 54) in PMMA. Also, the band at 1454 cm^{-1} can be attributed to the bending vibration of the C–H bonds of the –CH$_3$ group.[50,55,56] In the FT-IR spectrum of CM and CM/PMMA cryogel (Fig. 2), the peaks at 1066 cm^{-1} and 1257 cm^{-1} correspond respectively to glycosidic linkage and sulfate ester groups, and the two well-defined bands at 927 cm^{-1} and 844 cm^{-1} indicating the presence of 3,6-anhydro-D-galactose and D-galactose-4-sulfate. The peak observed at 850–840 cm^{-1} confirms the absence of λ-carrageenan.[57–59] The absorption band perceived at 3400 cm^{-1} is
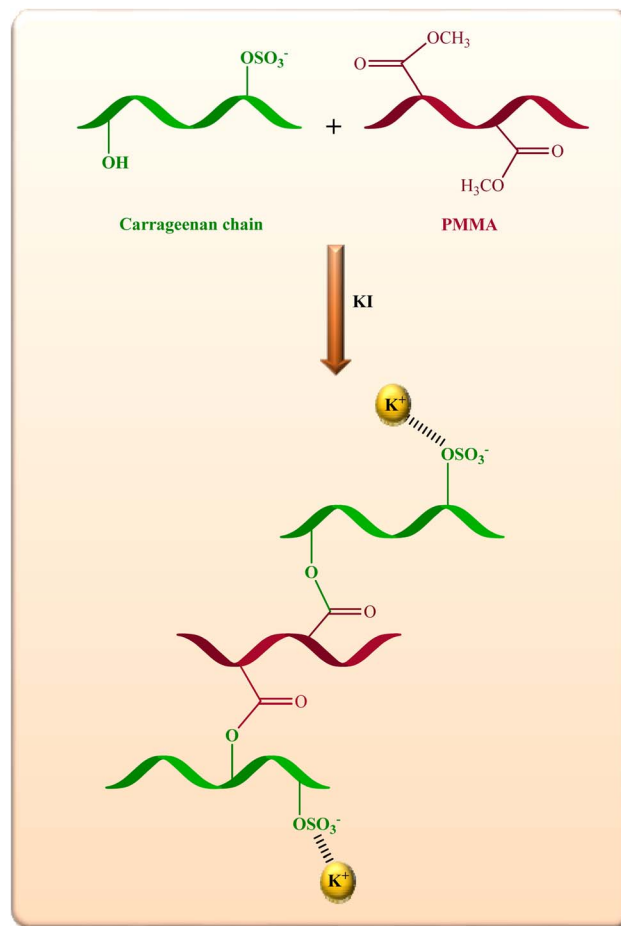

Fig. 1 Schematic pathway for preparation of hybrid CM/PMMA.

related to the O–H stretching mode, and the absorption band at 1650 cm^{-1} may be due to the water absorbed inside the CM. Additionally, the absence of ι-carrageenan is confirmed by the nonappearance of the absorption band at 805–800 cm^{-1}.[60,61] Comparison of the spectrum of CM, pure PMMA, and hybrid CM/PMMA revealed the broad and intense bands centered at 1735 cm^{-1}, 1149 cm^{-1} and 991 cm^{-1} are attributed to carboxyl group of PMMA grafting of PMMA onto CM backbone. Thus, the presence of these bands and decrease in intensity of O–H bending vibration in the spectrum of CM prove that PMMA was grafted onto O–H site of the CM through carrageenan macromolecule. Also, hydrogen bonding between hydroxyl groups can be strengthened in the gel network.

3.2 XRD of CM/PMMA hybrid cryogel

The crystal structures of pure PMMA, CM and CM/PMMA hybrid cryogel were evaluated using XRD analysis (Fig. 3). The XRD patterns of pure PMMA displayed two broad peaks at $2\theta = 13.8°$, $30.0°$, and that of CM one broad peaks at $2\theta = 22.5°$ describing their amorphous phase.[62–64] In the XRD pattern of CM/PMMA cryogel, the peaks at $2\theta = 24.76°$, $24.20°$, $35.92°$, $42.38°$, $44.39°$, $51.69°$, $56.79°$, $58.35°$, $64.57°$, $68.99°$ correspond to the (111), (200), (220), (311), (222), (400), (331), (420),
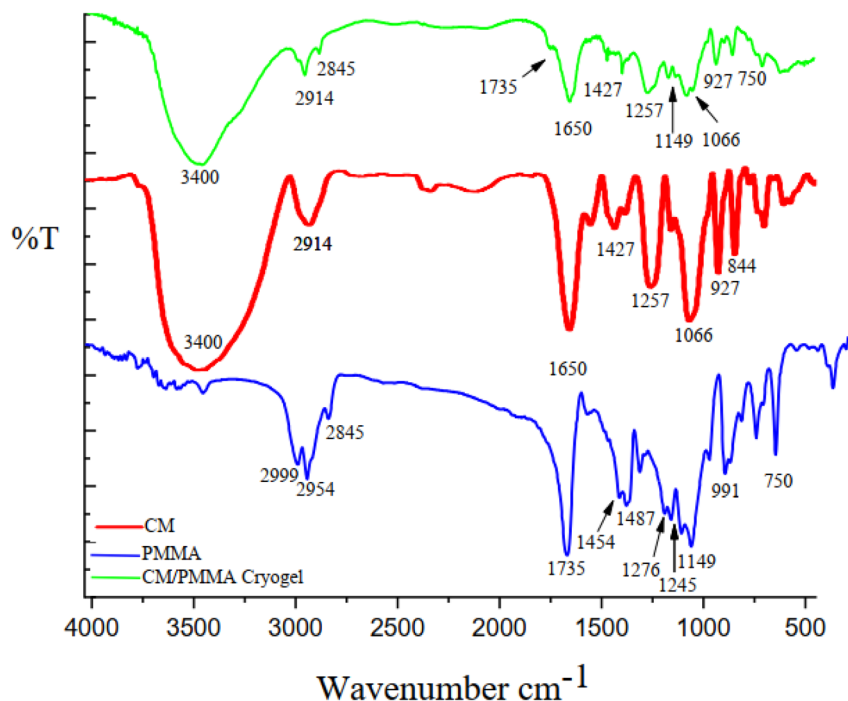
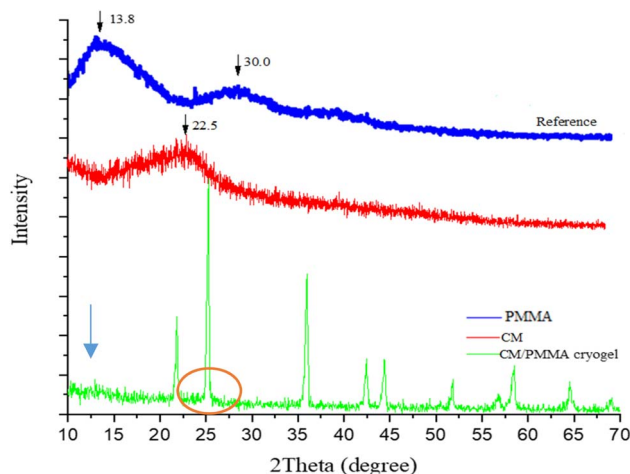Fig. 2   FTIR spectrum of CM/PMMA, CM and PMMA.

Fig. 3   The XRD pattern for pure PMMA, CM, and CM/PMMA cryogel.

(442) and (511) crystal planes of a cubic system of KI, according to the standard powder diffraction card of Joint Committee on Powder Diffraction Standards (JCPDS): [00-004-0471]. This indicated that the KI was not wholly removed during successive washing and was trapped in the cryogel pores. The disappearance or less intensified peaks, in the CM/PMMA cryogel compared to its components CM and PMMA, indicates the presence of interaction between the components.[65] The peaks attributed to amorphous PMMA and CM have a very low intensity in the XRD pattern CM/PMMA and are hidden by the intense and narrow peaks of the cubic crystal structure of KI.[66–69]

3.3   UV-vis spectrum

Fig. 4a shows UV-vis diffuse reflectance spectrum (expressed as absorbance) of CM, PMMA, and CM/PMMA cryogel. The absorption bands at 234 nm in the PMMA spectra were attributed to the $\pi \rightarrow \pi^*$ transition of carbonyl group. The UV-visible spectrum of CM shows a sharp peak at 225 and 216 nm.[70] The appearance of two new peaks at 301 and 370 nm indicated the presence of interaction between CM and PMMA. The estimation of the energy of the optical band gap (E_g) can be carried out using Kubelka–Munk theory[71] according to the Tauc model expressed as follows:

$(\alpha \hbar v)^2 = \hbar v - E_g$, with $\alpha = -1/t \ln T$, and $T = 10^{-A}$, where $\hbar$ represent the Planck constant, A is the absorbance, v is the frequency, α is the absorption coefficient, T is the transmittance, t for thickness, and E_g. energy gap. According to the results displayed in Fig. 4b, it is clear that the interaction between CM and PMMA leads to a decrease of the band gap from 3.4 eV and 1.9 eV to 1.6 eV.

3.4   TGA analysis

Thermogravimetric analysis was also carried out for CM/PMMA hybrid cryogel under argon, and oxygen atmosphere, and different TGA curves, as a function of different atmospheres were obtained as shown in Fig. 5. TGA analysis revealed that CM/PMMA hybrid cryogel shows different pyrolysis and combustion behavior under oxidative (air) and non-oxidative atmosphere. In the case of CM/PMMA hybrid cryogel on oxygen atmosphere, three-step weight loss occur while thermal decomposition under argon atmosphere is two-step weight loss. In the presence of the oxidative atmosphere,
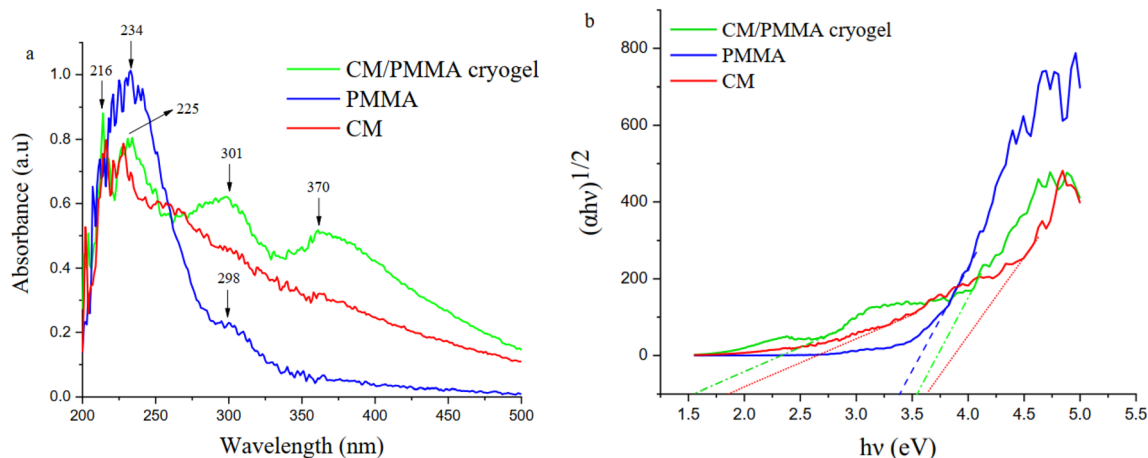
Fig. 4 (a) UV-vis and (b) band gap diagram of CM, PMMA, and CM/PMMA hybrid cryogel C.
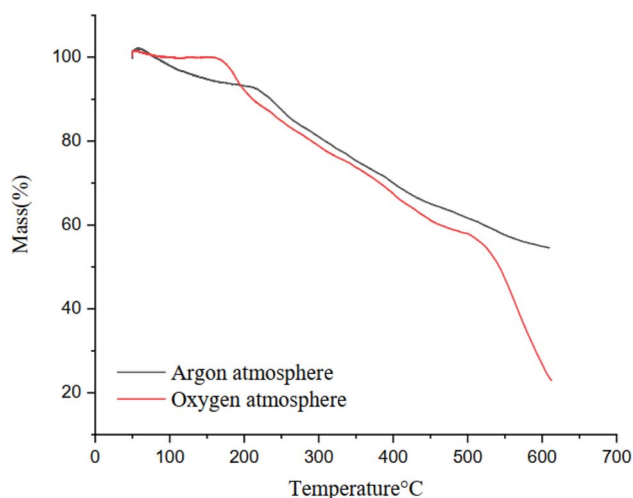

Fig. 5 TGA of CM/PMMA hybrid cryogel in argon and oxygen atmosphere.

the mass loss (78%) is higher than in the argon atmosphere (42%). These results are consistent with previous research and may be due to the decomposition of the polysaccharide structure of CM in oxidative atmosphere.[72] In argon atmosphere, small weight loss was observed in the first step from 50 to 280 °C, which is mainly due to the elimination of moisture from the cryogel. Most of the weight loss due to pyrolysis occurs in step 2 (300–800 °C), due to the breakdown of carbohydrates and release of the volatiles. Because the thermal degradation of CM and PMMA under oxidative atmosphere occurs in the ranges of 100–200 °C (ref. 64) and 300–400 °C (ref. 73) respectively, so the step observed in 600–800 °C is evident that grafting PMMA on CM has modified the thermal property of CM.[74] In the third stage (600–800 °C), the vaporization of carbonaceous materials, and gasification occurred and the loss in weight is principally due to the formation of synthesis gas.

3.5 BET analysis

The thermal conductivity is strongly influenced by the surface properties of the adsorbent, such as nature and surface area.[75,76] Meanwhile, the pore size is affected by thermal conductivity. The nanosize pores could significantly inhibit heat transfer.[77] The surface properties of the CM/PMMA hybrid cryogel were analyzed by N_2 adsorption and desorption isotherms and are shown in Fig. 6. Textural properties, such as the specific surface area, pore volume, and pore size of the CM/PMMA hybrid cryogel are summarized in Fig. 6. The N_2 adsorption–desorption isotherms are of type IV, with hysteresis loops of type H3 as classified by IUPAC.[78,79] The pore diameter size of the CM/PMMA hybrid cryogel was found to be 4.46 nm which is greater than 2 nm, and hence confirms the mesoporous structures of the CM/PMMA cryogel.

3.6 Surface morphological analysis

The surface morphology of the cryogels was observed at different scales, as shown in Fig. 7. The results of the FTIR and BET investigation are closely linked with those of the FE-SEM analysis. CM/PMMA hybrid cryogel FE-SEM shows the three-dimensional and porous structure of the sheets. FE-SEM analysis of the surface morphology shows that the cryogel has a tight, dense, rough, and wavy surface, which indicates its high toughness and dense cross-linking, as shown in Fig. 7, the CM/PMMA hybrid cryogel has a porous surface with a range size of 37.65 μm to 65.86 μm. The images show the integrated structure that confirms the formation of a chemical bond.

3.7 Observation of self-healing process

To examine the self-healing property of the CM/PMMA cryogel, two circular samples impregnated with rhodamine B and methylene blue were prepared and then cut into two semi-circular parts. The two semicircular pieces of cryogel were joined and kept at 40 °C for 15 min (Fig. 8a–c). The self-healing process of the cryogel was monitored by recording the optical microscopy images before and after the self-healing. Fig. 8d–f
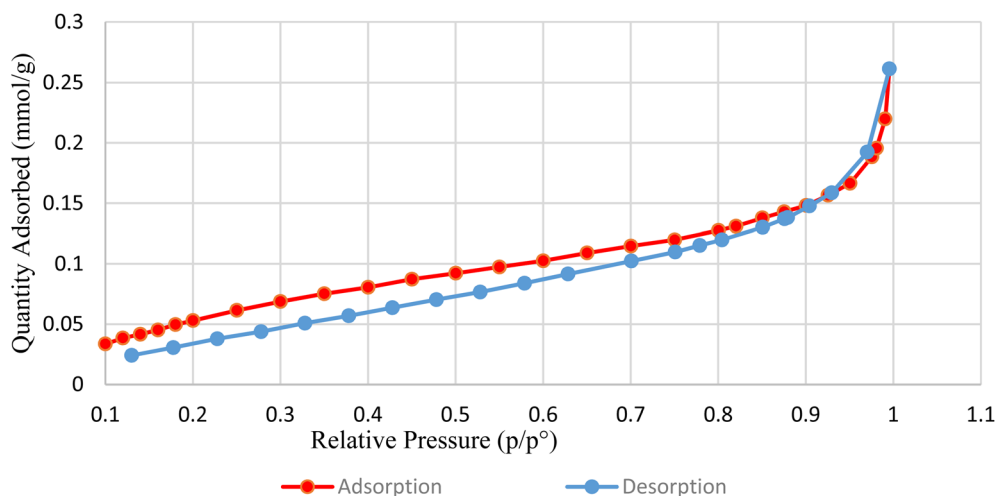
BET analysis for CM/PMMA cryogel

Fig. 6 Isotherm BET analysis of CM/PMMA cryogel.

showed that the cryogel possessed a good self-healable ability. The initial crack of the cryogel narrowed in 5 minutes and completely disappeared after 15 minutes.

The excellent self-healing ability of cryogel was observed, which could be due to two reasons: firstly, it should be noted that CM contains carrageenan supramolecular, and the interaction between sulfate and hydroxyl groups in the carrageenan supramolecular chains are affected to form hydrogen bonds and effectively binding the networks cryogel to each other.[80]

Certainly, hydrogen bonding is the most popular way to obtain supramolecular polymers and is considered as a reversible cross-linking.[81] The self-healing property was not observed at room temperature for a given time. Although an elevated temperature is not necessary for self-healing, it is believed that the release of carrageenan chains from a double helix structure at 40 °C would increase the mobility of the chain and accelerate the self-healing process. The double helices of carrageenan can be converted into coils during heating, and then the chains can
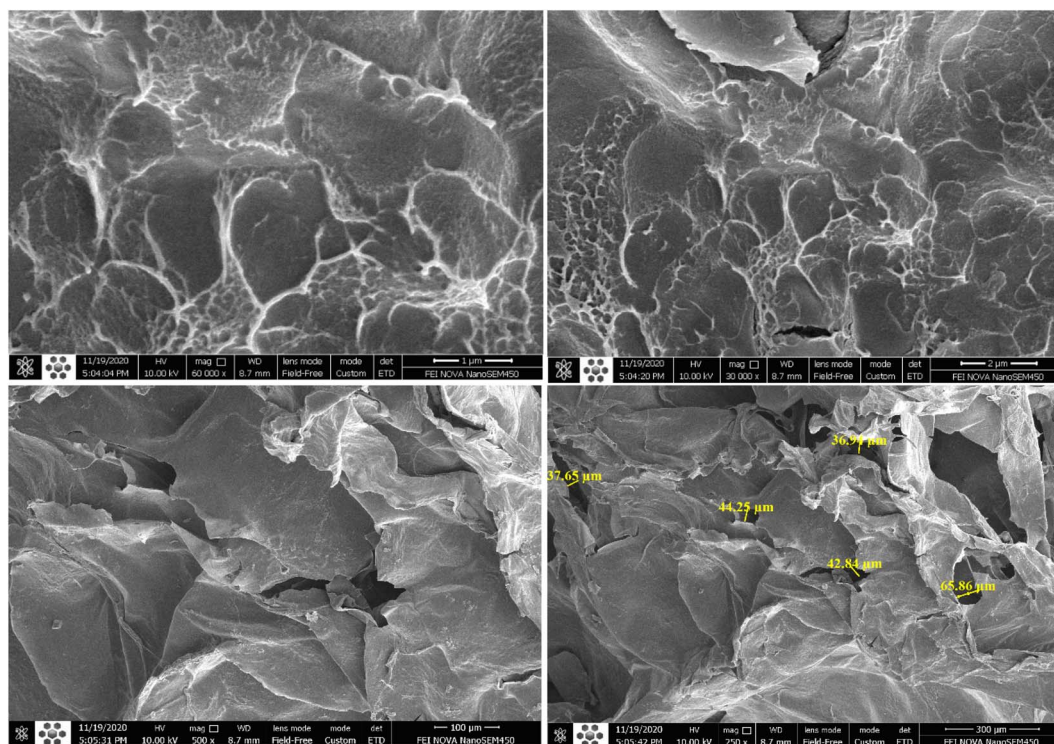

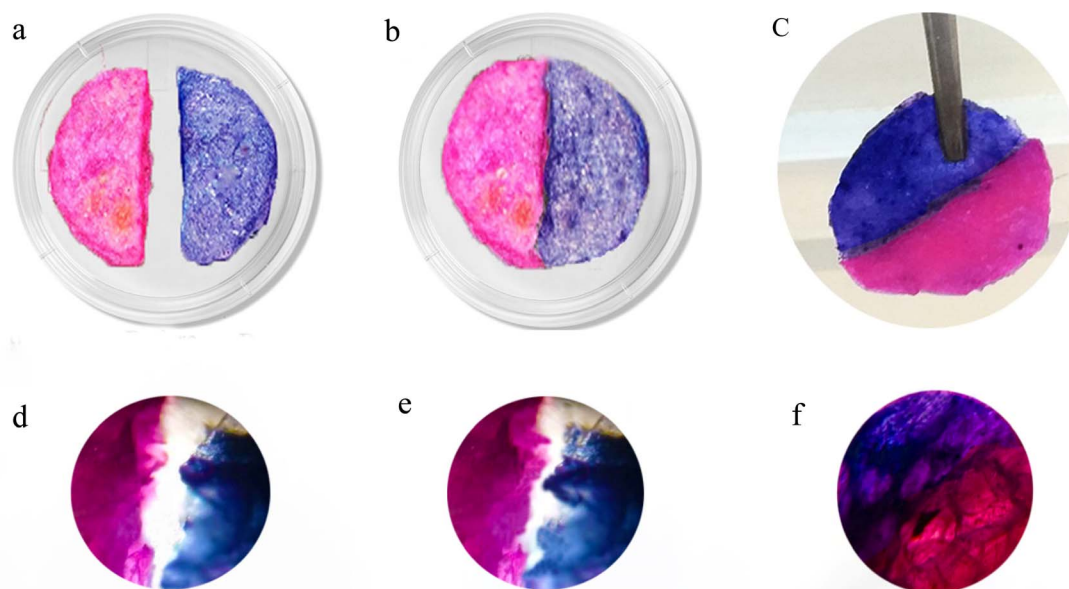Fig. 7 FE-SEM image of CM/PMMA cryogel.

Fig. 8 Self-healing CM/PMMA hybrid cryogel with an (a–c) semicircular, the images of the self-healing process were recorded by optical microscopy (d) 0 minutes (e) 10 minutes (f) 15 minutes.

be re-associated into double helices after decreasing temperature.[82–84] Secondly, in the presence of K^+ ions in the network of CM/PMMA cryogel, carrageenan chains were reassembled and heating, and cooling processes led to reduced double helix aggregates. Therefore, the presence of K^+ in CM/PMMA hybrid cryogel leads to helical structural transition contributed to the excellent self-healing properties of cryogel.[83,84]

3.8 Swelling behavior

Fig. 9a–c show the temperature-dependent swelling behaviour of the CM/PMMA hybrid cryogel at different temperatures, from 20 to 60 °C. The phase transition of κ-carrageenan in various types of cation solutions such as Mg^{2+}, Ca^{2+}, Na^+, K^+, Li^+ and phase transition temperatures, rheological properties, and gel-network characteristics during sol–gel and gel–sol transitions of κ-carrageenan-salt solution was reported.[85,86] The sol–gel transition of κ-carrageenan in a solution of K^+ ion is estimated to be 62–75 °C.[85–87] The thermo-responsive cryogel was swollen below phase transition temperature (T_p) of κ-carrageenan and shrunken above T_p. In general, the T_p of temperature-sensitive polymer could be changed by grafting hydrophobic or hydrophilic matter into its chains. It was reported that polymerization with hydrophobic chain, could decrease T_p to down value as
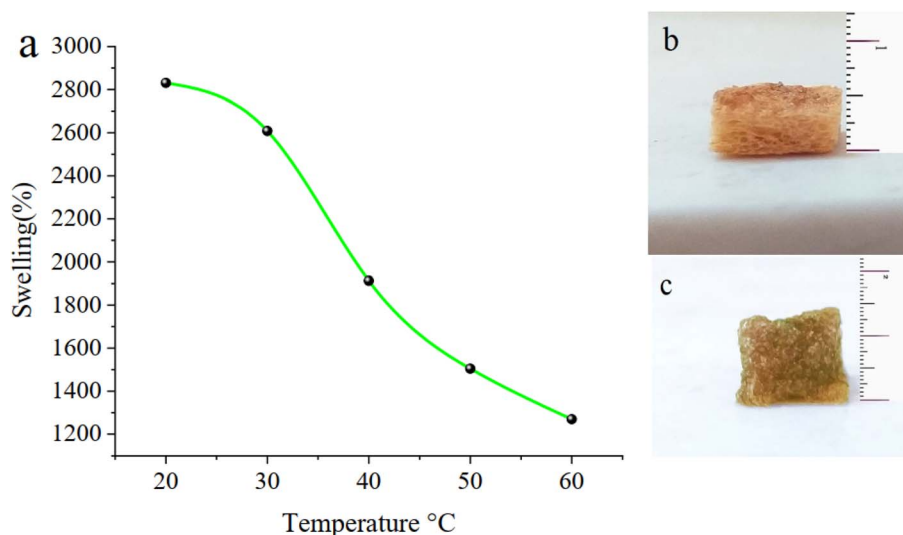

Fig. 9 (a) Temperature-dependent swelling behaviour of the CM/PMMA cryogel, (b) before and (c) after soaking in water.

well as their swelling properties.[77,88] So, grafting PMMA on CM leads to a decrease of T_p to 30 °C.

3.9 Mechanical properties

Density values were measured for all three insulators. As the thickness increases from 2.22 to 3.22, and 4.22 mm, the density increases from 0.42 to 0.55 and 0.7 g ml^{-1}, which is undoubtedly due to the lower porosity which also affects the mechanical properties.

The obtained CM/PMMA hybrid cryogel has shown unique mechanical properties. CM/PMMA hybrid cryogel is very light and flexible, which can be a good advantage for use as insulation and facilitate its transportation and use (Fig. 10a and b). Compressive experimental results show that the as-prepared CM/PMMA hybrid cryogel is extremely strong and tough. The results indicate that the mechanical properties improve with increasing thickness. CM/PMMA hybrid cryogel with 4.45 mm and 8.90 mm thickness can be compressed to a 4.6% and 10.5% height of the original cylinder samples without fracture, respectively. Fig. 10c express that when the thickness of the CM/PMMA hybrid cryogel increase, the compression strength of the CM/PMMA hybrid cryogel increases from 89.5% to 95.4% under compressive stress 0.08 MPa and 0.12 MPa respectively. According to the density trend and previous studies, the increase in density can be a confirmation of the reduction of porosity in the gel structure. Studies show that reducing porosity, or in other words, increasing density, leads to an increase in resistance. Therefore, probably due to the reduction of porosity with increasing thickness, the compressive strength increases.[89] This resistance to compression and the ability to recover to its original state upon decompression from elevated pressures makes the prototype aerogel blanket suitable for applications where high insulation, resistance to compression, and recovery after a compression.

3.10 Relationship between thickness and thermal conductivity

To achieve the relationship between thickness and thermal conductivity, the changes in thermal conductivity were investigated by increasing the thickness of the cryogel from 2.22 to 3.22, and 4.22 mm. The results indicated that the thermal conductivity increased as the thickness increased up to 4.22 mm (Fig. 11a). Fig. 11b displays, the linear relationship between the thermal conductivity and the thickness ($y = 0.0316x - 0.0180$). Studies show that by reducing the porosity of the material and increasing the density, the thermal conductivity of the material increases. One of the effective factors in the conductivity of materials is the presence of air holes in their structure. Previous researchers have reported that the presence of air holes improves the performance of materials as thermal insulation. The data obtained from the density measurement confirm that by increasing the thickness of the prepared insulation, the density of the material increases and the air voids decrease, which can lead to an increase in thermal conductivity.[90,91] According to the data obtained from the density measurement, we assume that the process of increasing the thermal conductivity is normal.

Generally, insulation materials have thermal conductivity less than 0.2 W m^{-1} K^{-1}. For example, a thermal conductivity of 0.114 and 0.096 W m^{-1} K^{-1} is reported for calcium silicate aerogel. Such reports of the thermal conductivity of hydrogels such as chrome leather scraps (0.383 to 0.190 W m^{-1} K^{-1}), silica aerogel (0.05 W m^{-1} K^{-1}) and *etc.*[92–94] Therefore, CM/PMMA hybrid cryogel shows suitable behaviour as thermal insulation has low thermal conductivity. A comparison of these results with the previous research indicates that CM/PMMA hybrid cryogel has good thermal insulation performance and can effectively avoid heat loss to the environment.
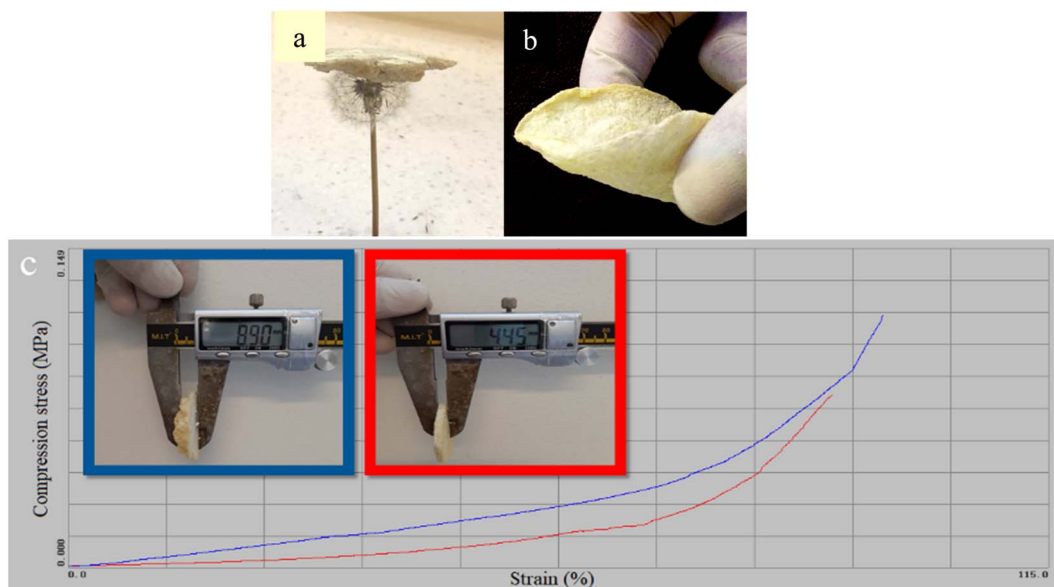

Fig. 10 Mechanical properties of CM/PMMA cryogel, (a) lightness, (b) flexibility and (c) compression test diagram.
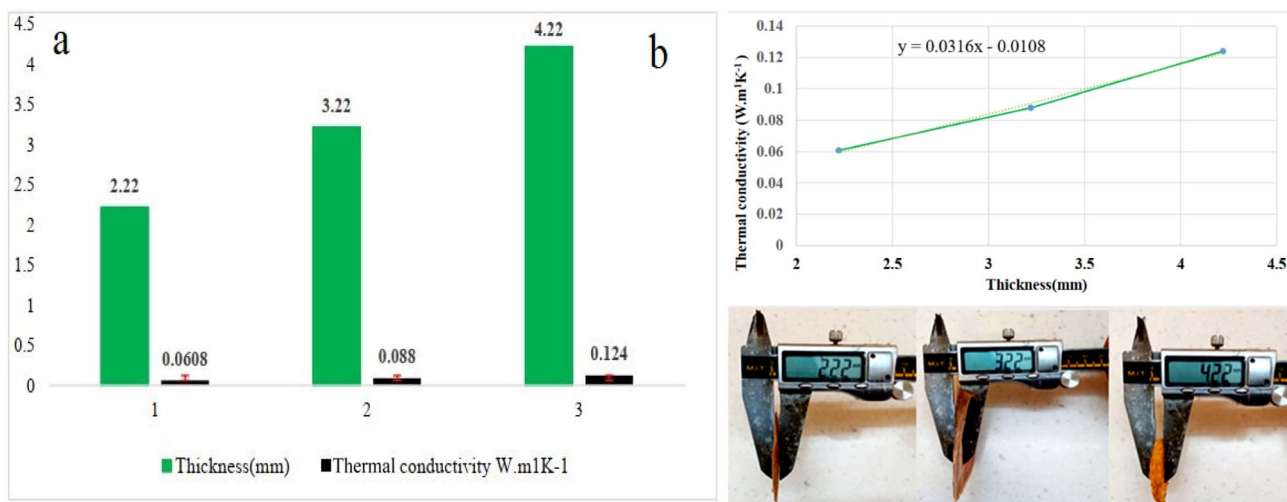
Fig. 11 (a) Relationship between thickness and thermal conductivity, (b) optimum thickness as a function of thermal conductivity for CM/PMMA cryogel.

In addition, the CM/PMMA hybrid cryogel did not ignite under flame exposure. Materials offering complete thermal insulation due to their low thermal conductivity are not necessarily flame resistant, despite their high melting temperature. Flame retardancy is an advantage for materials with low thermal conductivity, which can ensure safety and longevity during the fire. The association of these characteristics suggests promising prospects for the using the CM/PMMA hybrid cryogel in the field of fire protection as a renewable flame-retardant material. To investigated the burning behaviour of CM/PMMA hybrid cryogel, the horizontal burning test was performed in which the sample is placed horizontally over a spirit lamp (Fig. 12). The results showed that CM/PMMA hybrid cryogel does not burn after removal of the flame, in all three ignition
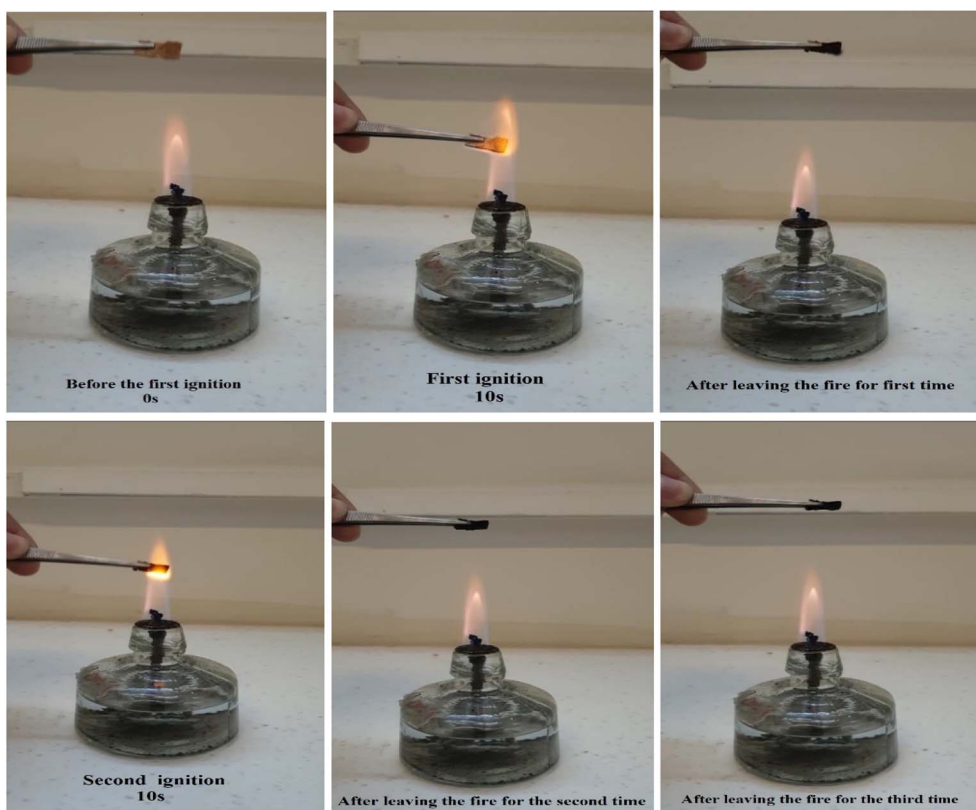

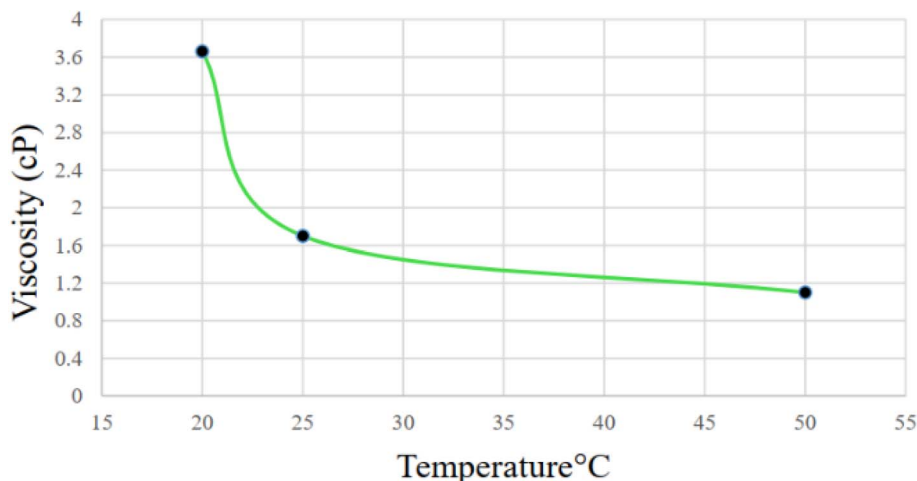**Fig. 12** Flame retardancy test of CM/PMMA cryogel.

Fig. 13 Dependence of CM solution viscosity on temperature.

processes, does not drain flaming particles, and nor produces smoke, which confirms the excellent flame-retardant properties. The test data tabulated in Table SI1 (see ESI†) revealed that CM/PMMA hybrid cryogel is capable of passing the horizontal burning test. It was also observed that burning leads to the formation of a layer of char on its surface. The formation of a char layer on the surface of CM/PMMA hybrid cryogel can effectively prevent further combustion and reduce the risk of material ignition.[95,96]

3.11 Viscosity measurements

Viscosity is one of the physical properties of CG solution, which depends on temperature, concentration and, type of CG.[97–100] Fig. 13 displays how the viscosity CM solution exponentially decreases with an increase in temperature. With decreasing temperature from 50 °C to 25 °C and 20 °C, the viscosity increased from 1.1 cP to 1.7 cP and 3.66 cP, respectively. This temperature dependence is consistent with previous research.[97,99] As the temperature decreases below 25 °C, a sol–gel transfer occurs, which leads to an increase in viscosity.

4 Conclusion

Novel light weight microporous cryogels with low thermal conductivity and flame-retardant properties were prepared from biocompatible and natural polymers CM and PMMA. The dual cross-linking strategy, including covalent binding between CM and PMMA and electrostatic interaction between K$^+$ and carrageenan sulfate group was used to prepare CM/PMMA cryogels with improved mechanical properties and stability. Investigation of mechanical, thermophysical, and physicochemical properties of the obtained cryogel shows that CM/PMMA hybrid cryogel has good flexibility and self-healing ability at low temperatures. We found that there is a linear relationship between thermal conductivity and CM/PMMA cryogel thickness. This halogen and phosphorus-free flame resistant cryogel represent a chief improvement due to its low toxicity. These features increase the lifetime of the insulator and the possibility of extending its use in buildings, clothing and coating.

Conflicts of interest

There are no conflicts to declare.

References

1 Z. Y. Wu, C. Li, H. W. Liang, J. F. Chen and S. H. Yu, *Angew. Chem.*, 2013, **125**, 2997–3001.

2 H. Yu, Z. Tong, B. Zhang, Z. Chen, X. Li, D. Su and H. Ji, *Chem. Eng. J.*, 2021, **418**, 129342.

3 Y. Nakanishi, Y. Hara, W. Sakuma, T. Saito, K. Nakanishi and K. Kanamori, *ACS Appl. Nano Mater.*, 2020, **3**, 49–54.

4 L. F. Su, L. Miao, S. Tanemura and G. Xu, *Sci. Technol. Adv. Mater.*, 2012, **13**, 035003.

5 Y. Kobayashi, T. Saito and A. Isogai, *Angew. Chem.*, 2014, **126**, 10419.

6 B. Wicklein, A. Kocjan, G. Salazar-Alvarez, F. Carosio, G. Camino, M. Antonietti and L. Bergström, *Nat. Nanotechnol.*, 2015, **10**, 277–283.

7 Y. Si, X. Wang, L. Dou, J. Yu and B. Ding, *Sci. Adv.*, 2018, **4**, eaas8925.

8 J. Koo, J. W. Kim, M. Kim, S. Yoon and J. H. Shim, *Int. J. Precis. Eng.*, 2021, **8**, 445–451.

9 X. Zhang, T. Zhang, Z. Yi, L. Yan, S. Liu, X. Yao, A. Guo, J. Liu and F. Hou, *Ceram. Int.*, 2020, **46**, 28561–28568.

10 H. Shaabani, S. Davoudizadeh, S. A. Shobeiri, S. Bahadorikhalili and K. Khezri, *J. Therm. Anal. Calorim.*, 2019, 1–11.

11 G. Luo, X. Gu, J. Zhang, R. Zhang, Q. Shen, M. Li and L. Zhang, *J. Appl. Polym. Sci.*, 2017, **134**, DOI: **10.1002/app.44434**.

12 Y. Nie, I. T. Mugaanire, Y. Guo, R. Wang, K. Hou and M. Zhu, *Prog. Nat. Sci.: Mater. Int.*, 2021, **31**, 33–40.

13 F. Zou and T. Budtova, *Carbohydr. Polym.*, 2021, 118130.

14 V. D. Prajapati, P. M. Maheriya, G. K. Jani and H. K. Solanki, *Carbohydr. Polym.*, 2014, **105**, 97–112.

15 Z. Wang, B. Xiao, Z. Lin, Y. Xu, Y. Lin, F. Meng, Q. Zhang, L. Gu, B. Fang and S. Guo, *Angew. Chem.*, 2021, **133**, 23576–23581.

16 K. Ganesan and L. Ratke, *Soft Matter*, 2014, **10**, 3218–3224.

17 H. C. Yu, C. Y. Li, M. Du, Y. Song, Z. L. Wu and Q. Zheng, *Macromolecules*, 2019, **52**, 629–638.

18 G. Mahadevan and S. Valiyaveettil, *Chem. Res. Toxicol.*, 2021, **34**, 1468–1480.

19 F. Pahlevanzadeh, H. Bakhsheshi-Rad, M. Kharaziha, M. Kasiri-Asgarani, M. Omidi, M. Razzaghi, A. F. Ismail, S. Sharif, S. RamaKrishna and F. Berto, *J. Mech. Behav. Biomed. Mater.*, 2021, **116**, 104320.

20 M. Vedhanayagam, S. Anandasadagopan, B. U. Nair and K. J. Sreeram, *Mater. Sci. Eng., C*, 2020, **108**, 110378.

21 G. Wang, J. Zhao, G. Wang, L. H. Mark, C. B. Park and G. Zhao, *Eur. Polym. J.*, 2017, **95**, 382–393.

22 S. Estaji, A. Paydayesh, S. R. Mousavi, H. A. Khonakdar and M. M. Abiyati, *Polym. Compos.*, 2021, **42**, 5323–5334.

23 H. Li, L. Song, C. Sun, R. Li, Y. Fu, H. Zhang, A. Yang and H. Liu, *Sci. Eng. Compos. Mater.*, 2018, **25**, 1107–1114.

24 H. Li, C. Sun, R. Li, Y. Fu, L. Song, A. Yang and H. Liu, *J. Polym. Eng.*, 2018, **38**, 811–818.

25 Q.-F. Guan, H.-B. Yang, C.-H. Yin, Z.-M. Han, K.-P. Yang, Z.-C. Ling and S.-H. Yu, *ACS Mater. Lett.*, 2021, **3**, 243–248.

26 E. Lucchi, *Renewable Sustainable Energy Rev.*, 2018, **82**, 3077–3090.

27 B. P. Jelle, *Energy Build.*, 2011, **43**, 2549–2563.

28 J. E. Fernández, *Science*, 2007, **315**, 1807–1810.

29 L. Aditya, T. Mahlia, B. Rismanchi, H. Ng, M. Hasan, H. Metselaar, O. Muraza and H. Aditiya, *Renewable Sustainable Energy Rev.*, 2017, **73**, 1352–1365.

30 I. Van der Veen and J. de Boer, *Chemosphere*, 2012, **88**, 1119–1153.

31 L. Wang, S. Wu, X. Dong, R. Wang, L. Zhang, J. Wang, J. Zhong, L. Wu and X. Wang, *J. Mater. Chem. A*, 2018, **6**, 4449–4457.

32 L. Zeng, R. Yang, Q. Zhang, H. Zhang, K. Xiao, H. Zhang, Y. Wang, P. K. Lam and G. Jiang, *Environ. Sci. Technol.*, 2014, **48**, 12586–12594.

33 M. Venier, A. Salamova and R. A. Hites, *Acc. Chem. Res.*, 2015, **48**, 1853–1861.

34 G.-L. Wei, D.-Q. Li, M.-N. Zhuo, Y.-S. Liao, Z.-Y. Xie, T.-L. Guo, J.-J. Li, S.-Y. Zhang and Z.-Q. Liang, *Environ. Pollut.*, 2015, **196**, 29–46.

35 Z. L. Yu, N. Yang, V. Apostolopoulou-Kalkavoura, B. Qin, Z. Y. Ma, W. Y. Xing, C. Qiao, L. Bergström, M. Antonietti and S. H. Yu, *Angew. Chem., Int. Ed.*, 2018, **57**, 4538–4542.

36 H. Xiang, L. Li, W. Chen, S. Yu, B. Sun and M. Zhu, *Prog. Nat. Sci.: Mater. Int.*, 2017, **27**, 369–373.

37 X. Ao, X. Du, D. Yu, W. Wang, W. Yang, B. Sun and M. Zhu, *Prog. Nat. Sci.: Mater. Int.*, 2020, **30**, 200–207.

38 C.-L. Kim and D.-E. Kim, *Sci. Rep.*, 2017, **7**, 1–11.

39 J. Liu, H. Wang, P. Wang, M. Guo, S. Jiang, X. Li and S. Jiang, *Food Hydrocoll.*, 2018, **83**, 134–142.

40 A. Górska, A. Krupa, D. Majda, P. Kulinowski, M. Kurek, W. P. Węglarz and R. Jachowicz, *AAPS PharmSciTech*, 2021, **22**, 1–14.

41 Y. Tian, X. Zhang, X. Feng, J. Zhang and T. Zhong, *Carbohydr. Polym.*, 2021, 118498.

42 T. W. Lin and S. h. Hsu, *Adv. Sci.*, 2020, **7**, 1901388.

43 E. P. o. F. Additives, N. S. a. t. Food, M. Younes, P. Aggett, F. Aguilar, R. Crebelli, M. Filipič, M. J. Frutos, P. Galtier, D. Gott and U. Gundert-Remy, *EFSA J.*, 2018, **16**, e05238.

44 L. Zhang, M. Tian and J. Wu, *Hydrogels with Self-Healing Attribute*, IntechOpen, 2016.

45 V. Naveen, A. P. Deshpande and S. Raja, *RSC Adv.*, 2020, **10**, 33178–33188.

46 V. Naveen, S. Raja and A. P. Deshpande, *Int. J. Plast. Technol.*, 2019, **23**, 157–169.

47 D. Zhao, X. Qian, X. Gu, S. A. Jajja and R. Yang, *J. Electron. Packag.*, 2016, 138.

48 W. R. Illeperuma, P. Rothemund, Z. Suo and J. J. Vlassak, *ACS Appl. Mater. Interfaces*, 2016, **8**, 2071–2077.

49 I. S. Tsagkalias, T. K. Manios and D. S. Achilias, *Polymers*, 2017, **9**, 432.

50 K. T. Arul, M. Ramanjaneyulu and M. R. Rao, *Curr. Appl. Phys.*, 2019, **19**, 375–380.

51 A. Singhal, K. Dubey, Y. Bhardwaj, D. Jain, S. Choudhury and A. Tyagi, *RSC Adv.*, 2013, **3**, 20913–20921.

52 D. Yu, J. Zhao, W. Wang, J. Qi and Y. Hu, *RSC Adv.*, 2019, **9**, 35532–35538.

53 Y. Liu, Y. Qin, R. Bai, X. Zhang, L. Yuan and J. Liu, *Int. J. Biol. Macromol.*, 2019, **134**, 993–1001.

54 S. V. Harb, M. C. Uvida, A. Trentin, A. O. Lobo, T. J. Webster, S. H. Pulcinelli, C. V. Santilli and P. Hammer, *Mater. Sci. Eng., C*, 2020, **110**, 110713.

55 G. Duan, C. Zhang, A. Li, X. Yang, L. Lu and X. Wang, *Nanoscale Res. Lett.*, 2008, **3**, 118–122.

56 Y. Li and H. Guo, *RSC Adv.*, 2020, **10**, 1981–1988.

57 A. Diharmi, D. Fardiaz, N. Andarwulan and E. S. Heruwati, *Phycol. Res.*, 2017, **65**, 256–261.

58 R. Chitra, P. Sathya, S. Selvasekarapandian and S. Meyvel, *Polym. Bull.*, 2020, **77**, 1555–1579.

59 H. M. Fahmy, A. A. Aly, S. M. Sayed and A. Abou-Okeil, *Polym. Adv. Technol.*, 2021, **32**, 1793–1801.

60 U. Andjelković, A. Milutinović-Nikolić, N. Jović-Jovičić, P. Banković, T. Bajt, Z. Mojović, Z. Vujčić and D. Jovanović, *Food Chem.*, 2015, **168**, 262–269.

61 N. A. A. Ghani, R. Othaman, A. Ahmad, F. H. Anuar and N. H. Hassan, *Arabian J. Chem.*, 2019, **12**, 370–376.

62 M. Hashem, M. F. A. Rez, H. Fouad, T. Elsarnagawy, M. A. Elsharawy, A. Umar, M. Assery and S. Ansari, *Sci. Adv. Mater.*, 2017, **9**, 938–944.

63 V. K. Thakur, D. Vennerberg, S. A. Madbouly and M. R. Kessler, *RSC Adv.*, 2014, **4**, 6677–6684.

64 S. Amirnejat, A. Nosrati, R. Peymanfar and S. Javanshir, *Res. Chem. Intermed.*, 2020, **46**, 3683–3701.

65 B. Gorain, H. Choudhury, M. Pandey, T. Madheswaran, P. Kesharwani and R. K. Tekade, in *Dosage form design parameters*, Elsevier, 2018, pp. 363–402.

66 R. Peymanfar, A. Javidan and S. Javanshir, *J. Appl. Polym. Sci.*, 2017, **134**, 45135.

67 R. Peymanfar, S. S. S. Afghahi and S. Javanshir, *J. Nanosci. Nanotechnol.*, 2019, **19**, 3911–3918.

68 R. Peymanfar, J. Karimi and R. Fallahi, *J. Appl. Polym. Sci.*, 2020, **137**, 48430.

69 X. Jian, B. Wu, Y. Wei, S. X. Dou, X. Wang, W. He and N. Mahmood, *ACS Appl. Mater. Interfaces*, 2016, **8**, 6101–6109.

70 A. Srivastava and R. Kumar, *Int. J. Carbohydr. Chem.*, 2013, 892615.

71 L. Pronti, J.-B. Mazzitelli, M. P. Bracciale, L. M. Rosati, C. Vieillescazes, M. L. Santarelli and A. C. Felici, *Spectrochim. Acta, Part A*, 2018, **200**, 10–19.

72 L. G. Fraga, J. Silva, S. Teixeira, D. Soares, M. Ferreira and J. Teixeira, *Energies*, 2020, **13**, 2756.

73 A. Yazdan, J.-Z. Wang, B.-K. Hu, W.-S. Xie, L.-Y. Zhao, C.-W. Nan and L.-L. Li, *Rare Met.*, 2020, **39**, 375–382.

74 K. Prasad, R. Meena and A. Siddhanta, *J. Appl. Polym. Sci.*, 2006, **101**, 161–166.

75 H. Babaei, A. J. McGaughey and C. E. Wilmer, *Chem. Sci.*, 2017, **8**, 583–589.

76 L. Wang, J. Feng, Y. Jiang, L. Li and J. Feng, *RSC Adv.*, 2019, **9**, 7833–7841.

77 X.-F. Sun, Q. Zeng, H. Wang and Y. Hao, *Cellulose*, 2019, **26**, 1909–1922.

78 I. Recommendations, *Pure Appl. Chem.*, 1982, **54**, 2201.

79 K. S. Sing, *Pure Appl. Chem.*, 1985, **57**, 603–619.

80 Y. Chen, C. Song, Y. Lv and X. Qian, *Polymer*, 2019, **184**, 121913.

81 S. K. Ghosh, *Self-healing materials: fundamentals, design strategies, and applications*, Wiley Online Library, 2009.

82 S. Liu and L. Li, *ACS Appl. Mater. Interfaces*, 2016, **8**, 29749–29758.

83 Z. Fan, L. Duan and G. Gao, *Sci. China Technol. Sci.*, 2020, 1–10.

84 Y. Deng, M. Huang, D. Sun, Y. Hou, Y. Li, T. Dong, X. Wang, L. Zhang and W. Yang, *ACS Appl. Mater. Interfaces*, 2018, **10**, 37544–37554.

85 S. Kara, E. Arda, B. Kavzak and Ö. Pekcan, *J. Appl. Polym. Sci.*, 2006, **102**, 3008–3016.

86 Y. Wang, C. Yuan, B. Cui and Y. Liu, *Carbohydr. Polym.*, 2018, **202**, 530–535.

87 V.-F. Lai, A.-L. Huang and C.-Y. Lii, *Food Hydrocolloids*, 1999, **13**, 409–418.

88 S. Ida, T. Kawahara, H. Kawabata, T. Ishikawa and Y. Hirokawa, *Gels*, 2018, **4**, 22.

89 M. R. de Moura, M. R. Guilherme, G. M. Campese, E. Radovanovic, A. F. Rubira and E. C. Muniz, *Eur. Polym. J.*, 2005, **41**, 2845–2852.

90 T. Shimizu, K. Matsuura, H. Furue and K. Matsuzak, *J. Eur. Ceram. Soc.*, 2013, **33**, 3429–3435.

91 A. M. Othman, M. M. Ghobashy, A. El-Sattar and E. Nour, *J. Sol-Gel Sci. Technol.*, 2021, **98**, 593–604.

92 B. P. Jelle, R. Baetens and A. Gustavsen, *The Sol-Gel Handbook*, ed. D. Levy and M. Zayat, 2015, pp. 1385–1412.

93 H. Xu, P. Xu, D. Wang, Y. Yang, X. Wang, T. Wang, W. An, S. Xu and Y.-Z. Wang, *Chem. Eng. J.*, 2020, **399**, 125781.

94 X. Ding, S. Wang, R. Dai, H. Chen and Z. Shan, *Environ. Technol. Innov.*, 2022, **25**, 102224.

95 N. Wang, H. Teng, F. Yang, J. You, J. Zhang and D. Wang, *Polymers*, 2019, **11**, 1708.

96 H. Li, Z. Hu, S. Zhang, X. Gu, H. Wang, P. Jiang and Q. Zhao, *Prog. Org. Coat.*, 2015, **78**, 318–324.

97 M. Şen and E. N. Erboz, *Int. Food Res. J.*, 2010, **43**, 1361–1364.

98 A. Bono, S. Anisuzzaman and O. W. Ding, *J. King Saud Univ. Eng. Sci.*, 2014, **26**, 3–9.

99 S. Iglauer, Y. Wu, P. Shuler, Y. Tang and W. A. Goddard III, *J. Pet. Sci. Eng.*, 2011, **75**, 304–311.

100 V. Lai, P. L. Wong and C. Y. Lii, *J. Food Sci.*, 2000, **65**, 1332–1337.